Mathematical and Computational Applications

MDPI

Article

Mathematical Analysis of Non-Steady-State Immobilized Glucose Dehydrogenase Glucose and Oxygen-Driven Reactions in Spherical Microreactors

Daniel Samuel [1,2], Mallikarjuna Mohanasundaraganesan [3] and Senthamarai Rathinam [1,*]

[1] Department of Mathematics, College of Engineering and Technology, SRM Institute of Science and Technology, Kattankulathur, Chennai 603203, Tamil Nadu, India
[2] P.G & Research Department of Mathematics, Cardamon Planters' Association College, Theni 625513, Tamil Nadu, India
[3] Department of Mathematics, Karpaga Vinayaga College of Engineering and Technology, Padalam 603308, Tamil Nadu, India
* Correspondence: senthamr@srmist.edu.in

Abstract

The governing reaction–diffusion model for carbohydrate oxidation catalyzed by an immobilized bienzyme system glucose dehydrogenase and laccase within a spherical porous microreactor is adapted from Baronas et al. and extended here to the non-steady-state regime. The model consists of coupled non-linear partial differential equations based on non-Michaelis–Menten kinetics. The principal novelty of this work lies in the derivation of closed-form semi-analytical expressions for transient and steady-state concentrations of the carbohydrate substrate, oxygen, and product, as well as for the effectiveness factor, using the Laplace Homotopy Perturbation Method (LHPM). The LHPM solutions are validated against MATLAB R2026a numerical simulations (maximum error $< 0.009\%$) and demonstrate superior accuracy compared to previously reported Adomian Decomposition Method (ADM) and Taylor Series Method (TSM) solutions. Parametric analysis reveals that the Thiele modulus, saturation parameters, and dimensionless time strongly influence the internal concentration profiles and reactor effectiveness. These analytical results provide rapid, closed-form predictive tools for optimizing catalyst particle size, enzyme loading, and operating conditions in immobilized enzyme microreactor systems.

Keywords: LHPM; microreactors; batch reactors; non-Michaelis–Menten kinetics; enzyme kinetics; reaction–diffusion; effectiveness factor

Check for updates

Academic Editor: Gianluigi Rozza

Received: 7 April 2026
Revised: 26 May 2026
Accepted: 27 May 2026
Published: 2 June 2026

Copyright: © 2026 by the authors. Licensee MDPI, Basel, Switzerland. This article is an open access article distributed under the terms and conditions of the Creative Commons Attribution (CC BY) license.

1. Introduction

Utilizing immobilized enzymes, MR enables unique substrate conversion with small volumes of the samples by reducing the cost alongside a minimum amount of processing time and system compactness [1,2]. The loss of enzyme activity due to immobilization is minimized by confining the enzymes within support materials, which helps stabilize their function [3]. To attain the maximum efficiency within the stirred tank reactor, an MR requires support materials that are resistant to the shear forces [4]. Due to their adjustable properties, the porous silica-based materials offer a promising solution that facilitates high enzyme loading [5].

Improvising the design for a highly efficient and productive biological process necessitates careful evaluation of various physical and biochemical parameters [1,6]. In many

MR systems, the presence of both solid and liquid phases makes mass transfer a key consideration [6,7]. The pores and particle sizes significantly affect the available surface area of the reactor, which majorly impacts the enzyme loading capacity [8]. Even though extensive physical experimentation is one method to optimize the effective working of the MR, advanced computational modeling offers an alternative approach by enabling the detailed simulation and analysis of bioreactor dynamics for further refinement [2].

Recently, many models have been developed representing the enzymatic reaction taking place in the batch reactor. Carvalho et al. [9] proposed a mathematical model representing the possibility of utilizing waste oils and fats in the production of biodiesel, and they have modeled the transfer reaction taking place in the batch reactor utilizing the Scilab application. Kushwaha et al. [10] has proposed a first-principle model by formulating and utilizing the non-steady-state mass balance and modifying them to attain realistic final conditions and incorporated fractional variable-order kinetics. Karthikeyan et al. [11] have modeled two chemical reactors: batch and continuous-stirred tank reactor in non-isothermal conditions, utilizing MATLAB and ASPEN PLUS for simulations. Mallikarjuna and Senthamarai [12] analyzed the mathematical model of reaction diffusion kinetics taking place in kinetically controlled cephalexin synthesis in a batch reactor with penicillin acylase immobilized in glyoxyl-agarose by implementing methods like Laplace Homotopy Perturbation Method for the non-steady-state and Adomian decomposition method for the steady-state dynamics. Mohammed et al. [13] identified and addressed the major limitation in current oxidative desulfurization models, such as their restricted suitability for industrial applications and the difficulties associated with scaling up the process while preserving high sulfur removal efficiency.

To the authors' knowledge, none of the existing literature provides a semi-analytical solution for the transient-state reaction–diffusion problem in a batch-stirred tank reactor utilizing an array of identical spherical porous microreactors with a bienzyme system. This study extends the reaction–diffusion model of Baronas et al. [2]—which describes carbohydrate oxidation catalyzed by a bienzyme glucose dehydrogenase/laccase system immobilized within carbon nanotubes—to the non-steady-state regime. The principal objective is to derive closed-form semi-analytical solutions using the Laplace Homotopy Perturbation Method (LHPM) and to analyze the effects of dimensionless time, radial distance, saturation parameters, and the Thiele modulus on microreactor performance. The model focuses on internal reaction–diffusion within the spherical microreactor particle under well-mixed bulk conditions; external mass transfer resistance is intentionally neglected as a first-phase approximation and will be incorporated in future work.

This study investigates the non-steady-state mathematical modeling of a stirred tank microreactor utilizing a dual-enzyme system—specifically, glucose dehydrogenase and laccase immobilized within carbon nanotubes based on the reaction–diffusion framework of Baronas et al. [2]. The governing equations are characterized by non-linear terms grounded in non-Michaelis–Menten kinetics. By employing the LHPM technique, we derive semi-analytical solutions for both non-steady-state and steady-state conditions. The validity of the non-steady-state results was corroborated through numerical simulations. Furthermore, the steady-state outcomes demonstrated superior accuracy, yielding lower error percentages than prior solutions [14] derived via the Adomian Decomposition Method (ADM) and Taylor Series Method (TSM). Additionally, the effectiveness factor of the microreactor was calculated to evaluate the influence of dimensionless time, saturation parameters, and the Thiele modulus.

These results have a direct application in the design and optimization of various biocatalytic systems used in industrial bioprocessing. The obtained semi-analytical results offer a valuable understanding of the biochemical system for predicting accurately and op-

timizing the transient behavior of enzyme-based microreactors. By capturing the transient dynamics of the reaction–diffusion process within a porous medium, the model enables the precise prediction of substrate conversion and enzyme efficiency over time. The enhanced understanding of the non-Michaelis–Menten kinetics and the effective working of the system under realistic conditions allows for improved control and scalability of bioreactors employing immobilized enzymes.

This article is organized as follows: Section 1 provides the introduction and novelty of the research work, and Section 2 provides the details and mathematical formulation of the considered model. In Section 3, the semi-analytical solutions of the governing equations are provided for both the non-steady-state and steady-state dynamics. These results are compared with the numerical simulation results in Section 4. The major findings of this research work is detailed in Section 5, succeeded by the concluding remarks in Section 6.

2. Mathematical Model and Governing Equations

The following coupled reaction–diffusion model is adapted from Baronas et al. [2], which describes carbohydrate oxidation catalyzed by a bienzyme glucose dehydrogenase/laccase system immobilized in a spherical porous microreactor with carbon nanotubes. The reaction kinetics follow the non-Michaelis–Menten framework, accounting for dual-substrate saturation and inhibition effects characteristic of coupled enzyme systems. The biochemical reaction sequence is:

$$S + E_1^{\text{ox}} \xrightarrow{k_1} P + E_1^{\text{red}}, \tag{1}$$

$$E_1^{\text{red}} \xrightarrow{k_2} E_1^{\text{ox}} + 2e^-, \tag{2}$$

$$E_2^{\text{ox}} + 4e^- \xrightarrow{k_3} E_2^{\text{red}}, \tag{3}$$

and

$$E_2^{\text{red}} + O_2 \xrightarrow{k_4} E_2^{\text{ox}} + 2H_2O. \tag{4}$$

In this context, S represents the carbohydrate substrate (e.g., glucose or cellobiose), O_2 denotes dissolved oxygen, and H_2O refers to water. E_1^{ox} and E_1^{red} denote the oxidized and reduced forms of the carbohydrate-oxidizing enzyme (Enzyme 1, e.g., glucose dehydrogenase); E_2^{ox} and E_2^{red} denote the oxidized and reduced forms of the oxygen-reducing enzyme (Enzyme 2, e.g., laccase). P is the reaction product. The rate constants k_1 and k_4 govern the substrate oxidation and oxygen reduction steps, respectively, while k_2 and k_3 govern the inter-enzyme electron transfer steps.

This reaction scheme represents a well-established coupled bienzyme architecture used in enzymatic fuel cells and amperometric biosensors [2]. Enzyme 1 oxidizes the carbohydrate substrate and releases electrons; these electrons are transferred to Enzyme 2 via direct electron transfer through the carbon nanotube support, consistent with the system described in Baronas et al. [2]. Enzyme 2 subsequently reduces dissolved oxygen, regenerating its oxidized form and closing the catalytic cycle. Oxygen is therefore a substrate for Enzyme 2 only, not for the carbohydrate-oxidizing Enzyme 1. Although glucose dehydrogenase requires NAD^+ or $NADP^+$ as a cofactor in free solution, the present model follows the framework of Baronas et al. [2] in which direct electron transfer via the carbon nanotube support serves as the electron-relay mechanism, effectively subsuming cofactor regeneration into the inter-enzyme electron transfer steps (Equations (2) and (3)) consistent with mediated bioelectrocatalysis. The model variable L used in subsequent equations represents the carbohydrate substrate concentration (labelled as in Baronas et al. [2] for consistency).

The stirred tank is assumed to be sufficiently well-mixed so that bulk concentrations L_b, O_b, and P_b are spatially uniform. Oxygen is assumed to be present at a uniform bulk

concentration O_b throughout the stirred tank, maintained by sufficient aeration of the reactor; the model does not explicitly account for oxygen mass-transfer limitations (k_La), which will be incorporated in future work. Consequently, the boundary conditions at the microreactor surface correspond to these constant bulk values. The present model focuses exclusively on internal reaction–diffusion within the spherical microreactor particle; external mass transfer resistance is intentionally neglected, which is valid for highly stirred systems where internal diffusion resistance dominates [8,9]. Incorporation of an external Nernst diffusion layer constitutes the next stage of this research. There is no energy transfer or enzymatic activity outside the MR. All dissolved components are uniformly distributed throughout the surrounding bulk medium beyond this diffusion zone.

Reaction–Diffusion Model

The governing equations are formulated by integrating Fick's second law with the bienzyme reaction kinetics, adapted from Baronas et al. [2]. The kinetic denominator structure arises from a quasi-steady-state analysis of the enzyme intermediate complexes in the bisubstrate Ping-Pong (substituted-enzyme) mechanism, in which each enzyme alternates between its oxidized and reduced forms as it processes successive substrates [2]. The model relies on mass conservation applied to each species inside the catalytic particle. The diffusion–reaction equations are:

$$\frac{\partial L_m}{\partial t} = D_{L,m}\left(\frac{\partial^2 L_m}{\partial r^2} + \frac{2}{r}\frac{\partial L_m}{\partial r}\right) - \frac{2V_L V_O L_m O_m}{K_O L_m V_L + 2K_L O_m V_O + L_m O_m V_L + 2L_m O_m V_O}, \tag{5}$$

$$\frac{\partial P_m}{\partial t} = D_{P,m}\left(\frac{\partial^2 P_m}{\partial r^2} + \frac{2}{r}\frac{\partial P_m}{\partial r}\right) + \frac{2V_L V_O L_m O_m}{K_O L_m V_L + 2K_L O_m V_O + L_m O_m V_L + 2L_m O_m V_O}, \tag{6}$$

$$\frac{\partial O_m}{\partial t} = D_{O,m}\left(\frac{\partial^2 O_m}{\partial r^2} + \frac{2}{r}\frac{\partial O_m}{\partial r}\right) - \left(\frac{V_L V_O L_m O_m}{K_O L_m V_L + 2K_L O_m V_O + L_m O_m V_L + 2L_m O_m V_O}\right), \tag{7}$$

along with the boundary conditions.

To maintain the symmetry of the system, a no-flux boundary condition is applied at the center of the microreactor (MR).

$$D_{S,m}\frac{dS_m}{dr}\Big|_{r=0} = 0, \quad S = L,\ P,\ O. \tag{8}$$

At the interface between the diffusion layer and the convective region ($r = R_1$), it is necessary to maintain continuity in the concentration values.

$$S_d(R_1) = S_b, \quad S = L,\ P,\ O, \tag{9}$$

In this context, $P_m(r)$ represents the product concentration formed within the microreactor (MR), while $L_m(r)$ and $O_m(r)$ denote the carbohydrate substrate and dissolved oxygen concentrations, respectively. The variable r refers to the radial coordinate in the spherical system of the MR.

To simplify the solution process, the following dimensionless parameters are introduced to non-dimensionalize the non-steady-state governing equations:

$$\begin{gathered}\tau = \frac{t}{R^2}, A(\chi) = \frac{L_m}{L_b},\ B(\chi) = \frac{O_m}{O_b},\ C(\chi) = \frac{P_m}{P_b},\ \chi = \frac{r}{R_1},\\ \phi_1^2 = \frac{R^2 V_L V_0}{D_{L,m}},\ \phi_2^2 = \frac{R^2 V_L V_0}{D_{P,m}},\ \phi_3^2 = \frac{R^2 V_L V_0}{D_{O,m}},\\ \alpha = V_L K_O L_b,\ \beta = O_b K_L V_O,\ \gamma = O_b L_b V_L,\ \sigma = V_O L_b O_b.\end{gathered} \tag{10}$$

The dimensionless saturation parameters α, β, γ, and σ are constructed from combinations of maximum reaction velocities, Michaelis constants, and bulk concentrations. These groups quantify the relative magnitudes of different kinetic terms in the non-Michaelis–Menten rate expression and determine whether the system operates in a quasi-linear

(first-order) regime, a saturated (zero-order) regime, or an intermediate transition zone. Since the Thiele moduli are defined as $\phi_i^2 = R^2 V_L / D_{S,m}$ (where i = 1, 2, 3), any change in pore structure that alters the effective diffusion coefficient $D_{S,m}$—such as reductions in pore diameter or particle porosity—directly increases ϕ_i^2 and thereby reduces the microreactor effectiveness factor η. The semi-analytical expressions derived here thus provide a rapid design tool for evaluating the impact of support material properties on reactor performance. The dimensionless form of the governing Equations (5)–(7) for the concentrations of carbohydrate substrate, product, and oxygen is derived as follows:

$$\frac{\partial A(\chi)}{\partial \tau} = \frac{\partial^2 A(\chi)}{\partial \chi^2} + \frac{2}{\chi}\frac{\partial A(\chi)}{\partial \chi} - \phi_1^2 \frac{2A(\chi)B(\chi)}{\alpha A(\chi)+2\beta B(\chi)+\gamma A(\chi)B(\chi)+2\sigma A(\chi)B(\chi)}, \tag{11}$$

$$\frac{\partial C(\chi)}{\partial \tau} = \frac{\partial^2 C(\chi)}{\partial \chi^2} + \frac{2}{\chi}\frac{\partial C(\chi)}{\partial \chi} + \phi_2^2 \frac{2A(\chi)B(\chi)}{\alpha A(\chi)+2\beta B(\chi)+\gamma A(\chi)B(\chi)+2\sigma A(\chi)B(\chi)}, \tag{12}$$

$$\frac{\partial B(\chi)}{\partial \tau} = \frac{\partial^2 B(\chi)}{\partial \chi^2} + \frac{2}{\chi}\frac{\partial B(\chi)}{\partial \chi} - \phi_3^2 \frac{A(\chi)B(\chi)}{\alpha A(\chi)+2\beta B(\chi)+\gamma A(\chi)B(\chi)+2\sigma A(\chi)B(\chi)}, \tag{13}$$

with modified boundary conditions, when $\tau = 0$

$$A(\chi,0) = 0,\ C(\chi,0) = 0,\ B(\chi,0) = 0, \tag{14}$$

when $\chi = 0$

$$\frac{\partial A}{\partial \chi} = 0,\ \frac{\partial C}{\partial \chi} = 0,\ \frac{\partial B}{\partial \chi} = 0 \tag{15}$$

when $\chi = 1$

$$A(\chi,\tau) = 1,\ C(\chi,\tau) = 1,\ B(\chi,\tau) = 1. \tag{16}$$

The system's effectiveness factor is expressed as

$$\eta = 3\int_0^1 \frac{rate(\chi,\tau)\chi^2}{rate_{surface}} \tag{17}$$

where

$$rate(\chi,\tau) = \frac{2AB}{\alpha A(\chi)+2\beta B(\chi)+\gamma A(\chi)B(\chi)+2\sigma A(\chi)B(\chi)}\ \ rate_{surface} = \frac{2}{\alpha+2\beta+\gamma+2\sigma} \tag{18}$$

3. Approximate Analytical Expressions of Carbohydrate Substrate, Oxygen, and Products

Non-linear equations are often used to describe complex phenomena across various disciplines, including physics, chemical engineering, biology, and applied mathematics. Obtaining solutions to these equations remains a constant difficulty for researchers in these domains. In recent years, multiple iterative strategies have been widely adopted to generate approximate analytical solutions for non-linear diffusion–reaction issues. The approaches include the Adomian Decomposition Method (ADM) [12], the Homotopy Perturbation Method (HPM) [15–17], the Homotopy Analysis Method (HAM) [17], the Variational Iteration Method (VIM) [18], and Taylor Series Method (TSM) [19], all of which are substantiated by comprehensive study and application.

One of the key strengths of the LHPM lies in its ability to function without relying on the assumption of a small parameter, which broadens its scope to encompass a wider range of non-linear systems. It has demonstrated significant effectiveness as an analytical approach for solving non-linear partial differential equations encountered in diverse areas such as gas dynamics, prey–predator interactions, fluid mechanics, and biochemical engineering.

In this study, the Laplace Homotopy Perturbation Method (LHPM) is applied to solve the transient-state non-linear reaction–diffusion equations given by Equations (11)–(13), with the boundary conditions (14)–(16). The Homotopy Perturbation Method (HPM), initially introduced by Ji-Huan He, is an effective approach for finding approximate analytical

solutions to highly non-linear differential equations. By integrating the Laplace transform with HPM, highly accurate results can be obtained across a large range of values using only a small number of repetitions [5,12,20]. A fundamental feature of the LHPM is that it does not rely on the presence of a tiny parameter, hence extending its applicability to a broader spectrum of non-linear situations. Recently, Mallikarjuna et al. [21,22] utilized the LHPM for solving the non-linear partial differential equation arising in immobilized enzyme systems, such as biosensor and batch reactors. This method has been utilized to solve non-linear differential equations arising in various fields, such as gas dynamics [23], prey–predator models [24], and fluid dynamics [25].

3.1. Semi-Analytical Expressions for the Non-Steady-State Solutions of Equations (11)–(13), Obtained Using the Laplace Homotopy Perturbation Method (LHPM)

For the concentration of the carbohydrate substrate (11), the approximate analytical expressions derived using LHPM (see Appendix A) is given as,

$$A(\chi,\tau) = \frac{\cosh\left(\chi\sqrt{\frac{L}{3}}\right)}{\cosh\left(\sqrt{\frac{L}{3}}\right)} - \pi\sum_{n=0}^{\infty}\frac{(2n+1)\cos\left(\frac{(2n+1)\pi}{2}\chi\right)e^{-3\tau\left(\frac{(2n+1)^2\pi^2}{4}+L\right)}}{\left(\frac{(2n+1)^2\pi^2}{4}+L\right)\sin\left(\frac{(2n+1)\pi}{2}\right)}, \tag{19}$$

for the concentration of the product (12), the approximate analytical expressions derived using LHPM (see Appendix A) is given as,

$$C(\chi,\tau) = \frac{\cosh\left(\chi\sqrt{\frac{O}{3}}\right)}{\cosh\left(\sqrt{\frac{O}{3}}\right)} + \pi\sum_{n=0}^{\infty}\frac{(2n+1)\cos\left(\frac{(2n+1)\pi}{2}\chi\right)e^{-3\tau\left(\frac{(2n+1)^2\pi^2}{4}+M\right)}}{\left(\frac{(2n+1)^2\pi^2}{4}+M\right)\sin\left(\frac{(2n+1)\pi}{2}\right)}, \tag{20}$$

for the concentration of oxygen (13), the approximate analytical expressions derived using LHPM (see Appendix A) is given as,

$$B(\chi,\tau) = \frac{\cosh\left(\chi\sqrt{\frac{N}{3}}\right)}{\cosh\left(\sqrt{\frac{N}{3}}\right)} - \pi\sum_{n=0}^{\infty}\frac{(2n+1)\cos\left(\frac{(2n+1)\pi}{2}\chi\right)e^{-3\tau\left(\frac{(2n+1)^2\pi^2}{4}+M\right)}}{\left(\frac{(2n+1)^2\pi^2}{4}+M\right)\sin\left(\frac{(2n+1)\pi}{2}\right)}, \tag{21}$$

where

$$L = \frac{2\phi_1^2}{\alpha+2\beta+\gamma+\sigma},\ N = \frac{\phi_3^2}{\alpha+2\beta+\gamma+\sigma},\ O = \frac{2\phi_2^2}{\alpha+2\beta+\gamma+\sigma} \tag{22}$$

3.2. Semi-Analytical Expression for the Steady-State Concentration Using the Laplace Homotopy Perturbation Method (LHPM)

At the peak, the MR reaches its equilibrium as a steady state by extending time period $\tau \to \infty$, wherein the system becomes time-independent and there is no change in the configuration of the system.

The obtained semi-analytical solutions for the steady-state concentrations of carbohydrate substrate and oxygen (19) and (21), as $\tau \to \infty$, are as follows:

$$A(\chi,\tau) = \frac{\cosh\left(\chi\sqrt{\frac{L}{3}}\right)}{\cosh\left(\sqrt{\frac{L}{3}}\right)}, \tag{23}$$

$$C(\chi,\tau) = \frac{\cosh\left(\chi\sqrt{\frac{O}{3}}\right)}{\cosh\left(\sqrt{\frac{O}{3}}\right)}, \tag{24}$$

and

$$B(\chi,\tau) = \frac{\cosh\left(\chi\sqrt{\frac{N}{3}}\right)}{\cosh\left(\sqrt{\frac{N}{3}}\right)}, \tag{25}$$

4. Semi-Analytical Result Validation

The non-linear diffusion Equations (11)–(13), along with the initial and boundary conditions Equations (14)–(16), are solved numerically using MATLAB's pdepe function. For both transient and steady-state scenarios, the approximate analytical solutions for the concentrations of carbohydrate substrate, product, and oxygen are derived using the Laplace Homotopy Perturbation Method (LHPM) as outlined in Equations (19) and (20) and (23)–(25). The accuracy of these analytical results is validated by comparing them with the numerical solutions, and the outcomes are presented graphically in Figure 1 for the transient dynamics. Table 1 represents the comparison of the semi-analytical expression with the numerical results, and Tables 2–4 represent the comparison of carbohydrate substrate, product, and oxygen concentrations obtained in the steady-state utilizing LHPM with the previous results from ADM and TSM. As shown in the tabulated data, the maximum deviation between the numerical solution and the LHPM is observed to be 0.0089% in the non-steady-state case, while the steady-state solution exhibits a maximum relative error of 0.00459%, which is much less than that of ADM (0.01133%) and of TSM (0.01432%). The results clearly indicate that the LHPM outperforms other semi-analytical methods for this particular model.

Table 1. Comparative evaluation of non-steady-state concentrations of carbohydrate substrate, product, and oxygen using numerical and semi-analytical solutions (19) and (20), for fixed parameters $\phi_1 = 0.5$, $\phi_2 = 1$, $\phi_3 = 0.7$, $\alpha = 0.5$, $\beta = 0.6$, $\gamma = 0.7$, and $\sigma = 0.5$, over varying τ.

	Carbohydrate Substrate $A(\chi)$			**Product $C(\chi)$**			**Oxygen $B(\chi)$**		
χ	**Numerical**	**LHPM**	**Error%**	**Numerical**	**LHPM**	**Error%**	**Numerical**	**LHPM**	**Error%**
0.0	0.99030	0.99090	0.06059	1.02000	1.02000	0.00000	0.99840	0.99810	0.03005
0.2	0.99069	0.99066	0.00256	1.01921	1.01928	0.00710	0.99846	0.99841	0.00515
0.4	0.99185	0.99114	0.07194	1.01683	1.01689	0.00598	0.99865	0.99861	0.00407
0.6	0.99380	0.99377	0.00249	1.01287	1.01292	0.00491	0.99897	0.99882	0.01499
0.8	0.99652	0.99653	0.00126	1.00732	1.00725	0.00696	0.99941	0.99944	0.00233
1.0	1.00001	1.00005	0.00378	1.00018	1.00019	0.00085	0.99999	0.99997	0.00149
Average Error%			0.00189			0.00198			0.00890

Table 2. Comparative evaluation of the LHPM results for the concentration of carbohydrate substrate Equation (23), with the previous results of ADM and TSM [14] for the fixed values of $\alpha = 0.5$, $\beta = 0.6$, $\gamma = 0.7$, $\sigma = 0.5$, $\phi_2^2 = 0.6$, $\phi_3^2 = 0.7$, and $\phi_1^2 = 0.5$ in steady-state.

	Concentration of Carbohydrate Substrate $A(\chi)$						
χ	**Numerical**	**ADM**	**Error%**	**TSM**	**Error%**	**LHPM**	**Error%**
0.0	0.97590	0.97560	0.03074	0.97570	0.02049	0.97585	0.00512
0.2	0.97687	0.97659	0.02852	0.97667	0.02012	0.97680	0.00717
0.4	0.97976	0.97955	0.02175	0.97958	0.01879	0.97969	0.00714
0.6	0.98458	0.98448	0.01011	0.98443	0.01587	0.98452	0.00609
0.8	0.99133	0.99140	0.00695	0.99123	0.01026	0.99131	0.00202
1.0	1.00000	1.00030	0.03028	1.00000	0.00038	1.00000	0.00000
Average Error%			0.00898		0.01432		0.00459

Table 3. Comparative evaluation of the LHPM results for the concentration of product Equation (24), with the previous results of ADM and TSM [14] for the fixed values of $\alpha = 0.5$, $\beta = 0.6$, $\gamma = 0.7$, $\sigma = 0.5$, $\phi_1^2 = 0.5$, $\phi_3^2 = 0.7$, and $\phi_2^2 = 0.5$ in steady-state.

	Concentration of Product $C(\chi)$						
χ	**Numerical**	**ADM**	**Error%**	**TSM**	**Error%**	**LHPM**	**Error%**
0.0	1.02400	1.02400	0.00000	1.02400	0.00000	1.02400	0.00010
0.2	1.02302	1.02303	0.00009	1.02303	0.00066	1.02303	0.00098
0.4	1.02010	1.02010	0.00052	1.02012	0.00256	1.02009	0.00098
0.6	1.01522	1.01524	0.00178	1.01527	0.00544	1.01532	0.00985
0.8	1.00838	1.00843	0.00470	1.00847	0.00885	1.00828	0.00992
1.0	0.99958	0.99968	0.01044	0.99970	0.01214	0.99970	0.01238
Average Error%			0.00292		0.00494		0.00207

Table 4. Comparative evaluation of the LHPM results for the concentration of oxygen Equation (25) with the previous results of ADM and TSM [14] for the fixed values of $\alpha = 0.5$, $\beta = 0.6$, $\gamma = 0.7$, $\sigma = 0.5$, $\phi_1^2 = 0.5$, $\phi_2^2 = 0.6$, and $\phi_3^2 = 0.5$ in steady-state.

	Concentration of Oxygen $B(\chi)$						
χ	Numerical	ADM	Error%	TSM	Error%	LHPM	Error%
0.0	0.98770	0.98780	0.01012	0.98780	0.01012	0.98770	0.00002
0.2	0.98819	0.98829	0.01017	0.98829	0.00946	0.98820	0.00101
0.4	0.98967	0.98977	0.01036	0.98974	0.00740	0.98966	0.00101
0.6	0.99213	0.99224	0.01089	0.99217	0.00427	0.99211	0.00202
0.8	0.99557	0.99569	0.01206	0.99558	0.00061	0.99567	0.01004
1.0	1.00000	1.00014	0.01435	0.99997	0.00282	0.99990	0.01000
Average Error%			0.01133		0.00484		0.00032

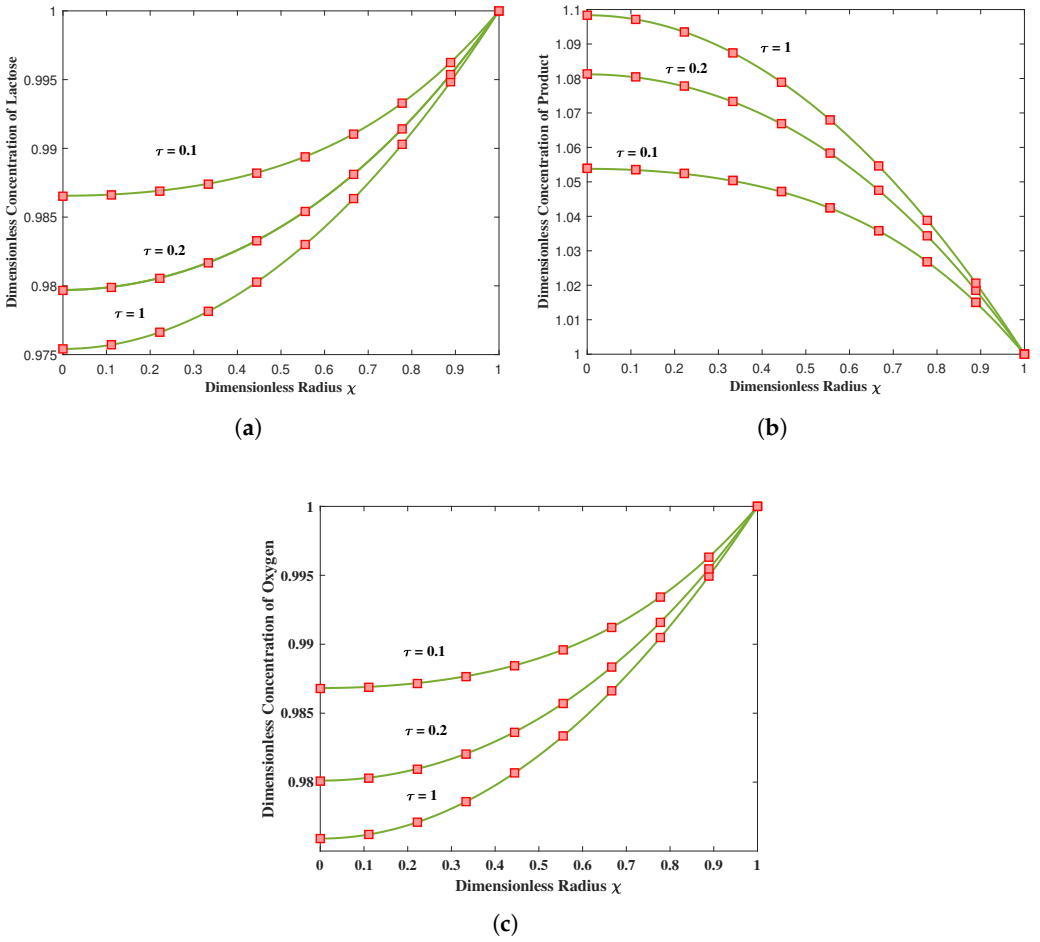


Figure 1. Dimensionless concentrations of (**a**) carbohydrate substrate, (**b**) product, and (**c**) oxygen versus the dimensionless radial distance χ, where "—" represents the numerical solutions, and "■■■" represents the LHPM solutions.

5. Results and Discussion

5.1. Influence of Enzyme Catalysis in the Spatial Domain

The dimensionless radial distance χ represents position within the immobilized microreactor, where $\chi = 0$ denotes the interior reaction zone, and $\chi = 1$ denotes the outer surface in contact with the bulk solution. From Figures 1 and 2, the concentrations of carbohydrate substrate and oxygen increase with radial distance because fresh substrate and dissolved oxygen diffuse inward from the bulk; the negative consumption terms in Equations (11) and (13) deplete these species near the center where enzymatic activity is greatest. Conversely, as shown in Figures 1b and 2c, the product concentration is highest at the interior ($\chi = 0$) and decreases toward the surface, since product is generated at the active catalytic core (positive production term in Equation (12)) and diffuses outward

into the bulk medium. This opposing spatial behavior is a direct consequence of the reaction–diffusion mechanism: the sign of the reaction term in Equations (11) and (12) determines whether a species is depleted or accumulated, ensuring that the region of greatest enzymatic activity (the catalytic core, $\chi \approx 0$) is simultaneously the region of lowest substrate concentration and highest product concentration—fully consistent with classical catalyst effectiveness theory. Since the Thiele moduli $\phi_i^2 = R^2 V_i / D_{i,m}$ link particle radius and effective diffusivity to reactor performance, a reduction in pore diameter (which lowers $D_{i,m}$) increases ϕ_i^2 and reduces η, illustrating directly how pore structure governs substrate conversion.

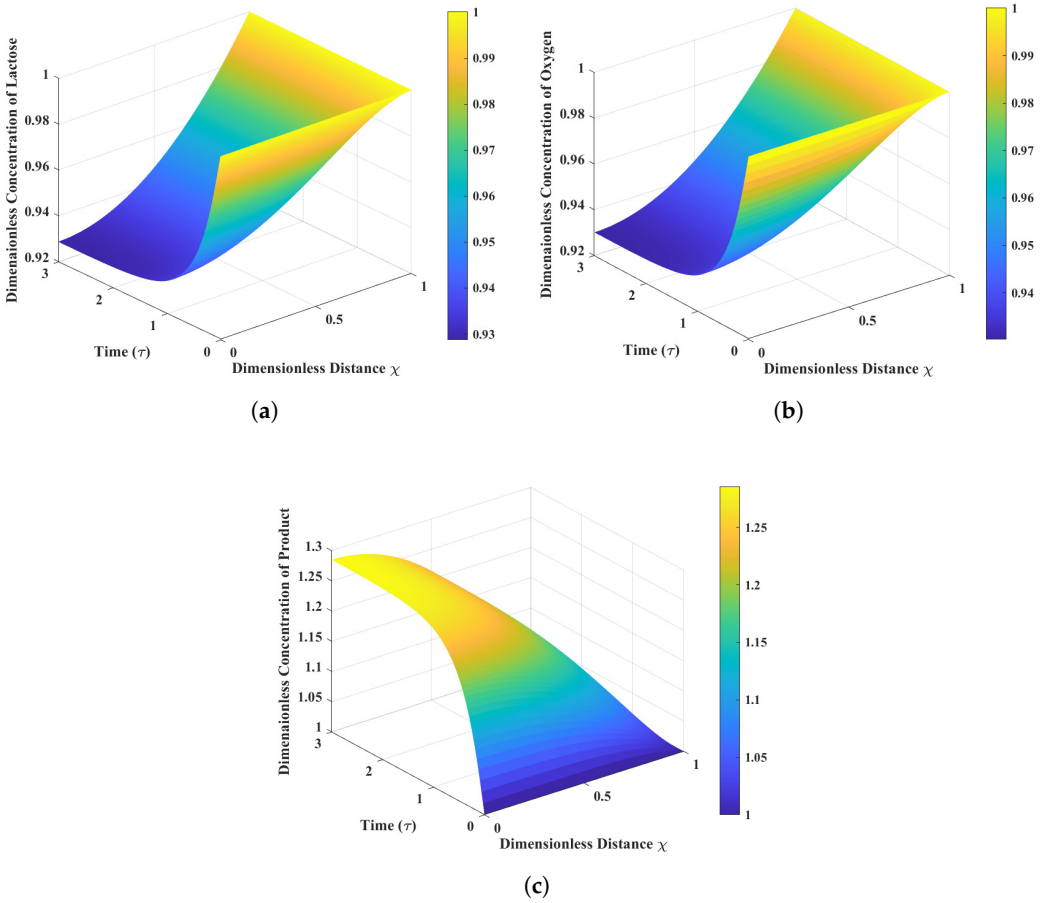


Figure 2. Surface plot representing the effect of dimensionless time τ and distance χ on the concentrations of (**a**) carbohydrate substrate, (**b**) oxygen, and (**c**) product.

5.2. Influence of Saturation Parameters on Enzymatic Reaction

The dimensionless saturation parameters α, β, γ, and σ are kinetic balance numbers that emerge from the non-dimensionalization of the dual-substrate enzymatic rate law. These parameters characterize the relative importance of linear Michaelis terms versus non-linear substrate–product interaction terms in the denominator of the kinetic expression. When $\alpha, \beta \gg 1$, the linear terms dominate, and the kinetics remain quasi-first-order; when $\gamma, \sigma \gg 1$, the non-linear product terms become significant, indicating the transition toward substrate saturation and zero-order behavior. When a parameter value exceeds unity, the system is in a saturated (near-zero-order) regime with respect to the corresponding species; when it is less than unity, the kinetics are in the linear (first-order) regime. In the unsaturated regime, an increase in the parameter values reflects a relative increase in substrate availability, which leads to higher substrate and oxygen concentrations throughout the microreactor while reducing product accumulation, since the reaction rate is not yet limited by substrate supply. As saturation increases (parameter ≥ 1), the kinetics transition toward

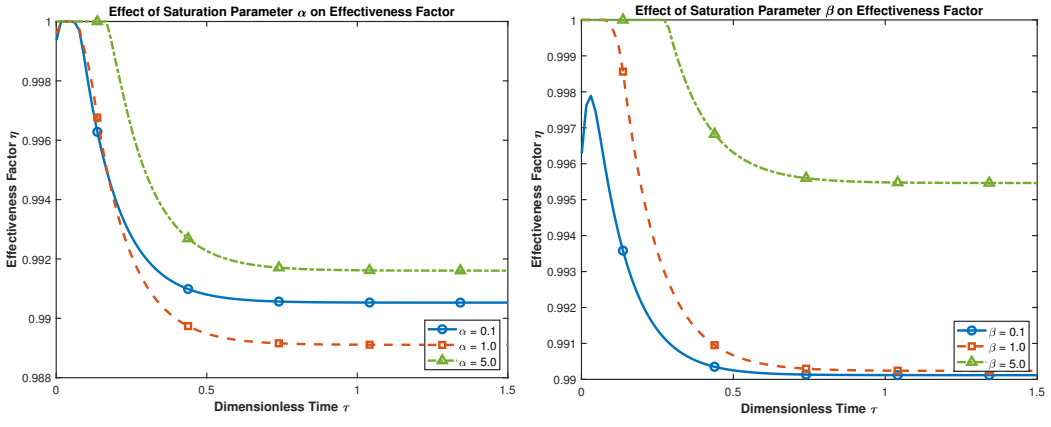
zero-order behavior and the spatial concentration profiles become progressively flatter. This flattening is evident when $\alpha \geq 100$, indicating near-uniform internal substrate distribution. Similar behavior is observed for β, γ, and σ.

5.3. Influence of Dimensionless Time τ

From Figures 1 and 2, it can be seen that as time increases, the concentrations of the carbohydrate substrate and oxygen decrease gradually and the system approaches a steady state at approximately $\tau \approx 1.5$. This reflects the progressive consumption of substrate by the enzymatic reaction as the system evolves from the initial condition. From Figure 2c, it is observed that the product concentration within the microreactor increases with time. At $\tau = 0$, no reaction has yet occurred, and no product is present. As the reaction proceeds, product concentration increases steadily, and the system reaches a quasi-steady state at $\tau \geq 1.5$, where the internal concentration profiles stabilize under the balance of diffusion and reaction. At this point, the internal substrate and product distributions remain constant in time; this is a steady-state profile, but not necessarily a complete conversion of all substrate in the microreactor.

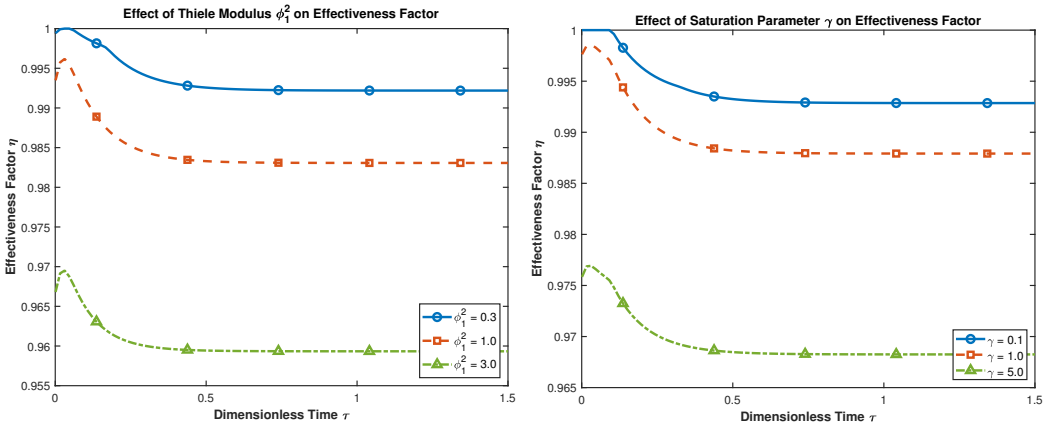
5.4. Evaluation of the System's Effectiveness Factor

The effectiveness factor η, expressed in Equation (17), is the ratio of the volumetric-average reaction rate within the catalytic pellet to the reaction rate evaluated at the surface concentration ($\chi = 1$). The effectiveness factor is in integral form to ensure consistency with heterogeneous reaction theory and to avoid ambiguity associated with local gradient-based formulations. By substituting the semi-analytical expressions of A and B in Equation (17), the effectiveness factor of the system is derived using MATLAB software. Figure 3a–d represent the effect of saturation parameters α, β, and γ and the Thiele modulus ϕ on the effective working of the system. From the subfigures, it can be seen that as the dimensionless time increases, the effectiveness factor first rises and then gradually approaches its equilibrium when $\tau \approx 0.8$. It can also be observed that as the saturation parameters α and β increase, the effectiveness factor increases, whereas when the Thiele modulus and γ increase, the effective working of the system decreases. Specifically, increasing α and β enhances catalytic effectiveness, while elevated ϕ and γ values reduce the system's performance, consistent with diffusion-limited kinetics.



(**a**) (**b**)

Figure 3. *Cont.*



(**c**) (**d**)

Figure 3. Effect of the saturation parameters α, β, and γ and the Thiele modulus.

6. Conclusions

This study presents a detailed transient reaction–diffusion analysis of a spherical porous microreactor immobilized with a bienzyme glucose dehydrogenase/laccase system operating under non-Michaelis–Menten kinetics. The governing reaction–diffusion model is adapted from Baronas et al. [2]; the principal contribution of the present work lies in extending that framework to the non-steady-state regime through the derivation of closed-form semi-analytical solutions using the Laplace Homotopy Perturbation Method (LHPM).

Closed-form approximate analytical expressions were successfully derived for the transient and steady-state concentrations of carbohydrate substrate, oxygen, and product, together with the effectiveness factor of the microreactor. The LHPM solutions show excellent agreement with MATLAB numerical simulations (maximum error $< 0.009\%$) and demonstrate superior accuracy compared to those previously reported in ADM and TSM solutions (Tables 2–4; LHPM error 0.00459% vs. ADM 0.01133% and TSM 0.01432%).

Parametric analysis shows that substrate and oxygen concentrations increase toward the outer surface of the microreactor due to diffusion from the bulk medium, while product concentration is highest near the catalytic core where the enzymatic reaction predominantly occurs. This is physically consistent with Equation (12), whose positive production term generates product internally, and Equations (11) and (13), whose negative consumption terms deplete substrates at the interior. Increasing diffusion limitations (higher Thiele modulus ϕ_2^2) reduces the effectiveness factor η, confirming that internal mass transport governs reactor efficiency.

The derived analytical expressions provide rapid, closed-form predictive tools for optimizing catalyst particle size, pore characteristics, enzyme loading, and operating conditions in immobilized enzyme bioreactor systems. The governing dimensionless parameters—Thiele moduli ϕ_i^2 and saturation parameters α, β, γ, and σ—can be determined from standard enzyme kinetic assays and pore characterization measurements, making the model directly applicable to experimental bioreactor design without requiring full numerical simulation. Future work will extend the model to include an external Nernst diffusion layer (external mass transfer resistance), enzyme deactivation, cofactor regeneration dynamics, and heterogeneous pore structures for more realistic industrial applications.

Author Contributions: Conceptualization, D.S. and S.R.; methodology, D.S. and S.R.; software, M.M.; validation, D.S., M.M. and S.R.; formal analysis, D.S. and S.R.; investigation, D.S.; resources, S.R.; data curation, D.S.; writing original draft preparation, D.S.; writing review and editing, S.R.; visualization, M.M.; supervision, S.R. All authors have read and agreed to the published version of the manuscript.

Funding: This research received no external funding.

Data Availability Statement: No new data were created or analyzed in this study. Data sharing is not applicable to this article.

Conflicts of Interest: The authors declare no conflicts of interest.

Nomenclature

Symbol	Definition
L_m, O_m, P_m	Dimensional concentrations of carbohydrate substrate, oxygen, and product inside the MR (mol m^{-3})
L_b, O_b, P_b	Bulk concentrations of substrate, oxygen, and product (mol m^{-3})
$A(\chi,\tau)$, $B(\chi,\tau)$, $C(\chi,\tau)$	Dimensionless concentrations of substrate, oxygen, and product
r	Radial coordinate (m)
R_1	Microreactor radius (m)
$\chi = r/R_1$	Dimensionless radial coordinate
t	Time (s)
$\tau = t/R^2$	Dimensionless time
$D_{l,m}$, $D_{o,m}$, $D_{p,m}$	Effective diffusion coefficients of substrate, oxygen, and product in MR (m^2 s^{-1})
V_L, V_O	Maximum reaction velocities for Enzymes 1 and 2 (mol m^{-3} s^{-1})
K_L, K_O	Michaelis constants for carbohydrate substrate and oxygen (mol m^{-3})
ϕ_1^2, ϕ_2^2, ϕ_3^2	Thiele moduli (dimensionless)
$\alpha = V_L K_O L_b$	Dimensionless saturation parameter (Kinetic parameter)
$\beta = O_b K_L V_O$	Dimensionless saturation parameter (Kinetic parameter)
$\gamma = O_b L_b V_L$	Dimensionless saturation parameter (Kinetic parameter)
$\sigma = V_O L_b O_b$	Dimensionless saturation parameter (Kinetic parameter)
η	Effectiveness factor (dimensionless)
k_1–k_4	Rate constants for enzyme reactions and electron transfer steps
E_1^{ox}, E_1^{red}	Oxidized and reduced forms of Enzyme 1 (carbohydrate dehydrogenase)
E_2^{ox}, E_2^{red}	Oxidized and reduced forms of Enzyme 2 (laccase)
MR	Microreactor
LHPM	Laplace Homotopy Perturbation Method
ADM	Adomian Decomposition Method
TSM	Taylor Series Method

Appendix A. LHPM-Based Approximate Solutions for Time-Dependent Concentrations of Carbohydrate Substrate, Oxygen, and Product

By constructing a homotopy for Equation (5), we obtain

$$(1-p)\left[\frac{\partial A}{\partial \tau} - \frac{\partial^2 A}{\partial \chi^2} - \frac{2}{\chi}\frac{\partial A}{\partial \chi} + \frac{\phi_1^2 2A\ (\chi=1)}{(\alpha+2\beta+\gamma+\sigma)}\right] + p\left[\frac{\partial A}{\partial t} - \frac{\partial^2 A}{\partial \chi^2} - \frac{2A}{\chi}\frac{\partial A}{\partial \chi} + \frac{\phi_1^2 A(\chi)\ B(\chi)}{\alpha A(\chi)+2\beta B(\chi)+\gamma A(\chi)B(\chi)+2\sigma A(\chi)B(\chi)}\right] = 0,$$

by implementing the boundary condition in

$$(1-p)\left[\frac{\partial A}{\partial \tau}-\frac{\partial^2 A}{\partial \chi^2}-\frac{2}{\chi}\frac{\partial A}{\partial \chi}+\frac{\phi_1^2\, 2A_0}{(\alpha+2\beta+\gamma+\sigma)}\right] + p\left[\frac{\partial A}{\partial t}-\frac{\partial^2 A}{\partial \chi^2}-\frac{A}{\chi}\frac{\partial A}{\partial \chi}+\frac{\phi_1^2 A_0\, B_0}{(\alpha+2\beta+\gamma+\sigma)}\right]=0. \tag{A1}$$

The approximation solutions are obtained and given below

$$A = A_0 + pA_1 + p^2A_2 + \cdots \tag{A2}$$

Substituting Equation (A2) into Equation (A1) and collecting terms of order p^0, we derive:

$$\frac{\partial A_0}{\partial \tau}-\frac{\partial^2 A_0}{\partial \chi^2}-\frac{2}{\chi}\frac{\partial A_0}{\partial \chi}+MA_0=0, \tag{A3}$$

where $M=\frac{2\,\phi_1^2}{\alpha+2\beta+\gamma+\sigma}$. The Laplace transform of Equation (A3) results in:

$$\frac{d^2\tilde{A}_0(\chi,s)}{d\chi^2}+\frac{2}{\chi}\frac{d\tilde{A}_0(\chi,s)}{dx}-(s+M)\tilde{A}_0(\chi,s)=0, \tag{A4}$$

incorporating the relevant boundary conditions,

$$\frac{d\tilde{A}_0(\chi,s)}{d\chi}=0 \text{ when } \chi=0, \tag{A5}$$

$$\tilde{A}_0(\chi,s)=\frac{1}{s} \text{ when } \chi=1, \tag{A6}$$

By applying AGM to hypothesize a solution for Equation (A4) that satisfies the initial as well as the boundary conditions in Equation (A5),

$$\tilde{A}_0(\chi,s)=A_0\cosh(lx)+B_0\sinh(lx), \tag{A7}$$

where $A_0=\frac{1}{\operatorname{scosh} l}$ and $B_0=0$, we obtained the solution for $\tilde{A}_0$ as

$$\tilde{A}_0(\chi,s)=\frac{\cosh(l\chi)}{\operatorname{scosh} l}. \tag{A8}$$

Applying Equation (A8) to Equation (A4), wherein $\chi=1$, we get

$$l^2+(2)\,l\tanh l\,-(s+L)=0, \tag{A9}$$

when l is sufficiently small, $\tanh l$ can be approximated by l; hence:

$$l=\sqrt{\tfrac{s+L}{3}}. \tag{A10}$$

Substituting this into Equation (A8) yields the solution of Equation (A4) as:

$$\tilde{A}_0(\chi,s)=\frac{\cosh\left(\chi\sqrt{\frac{s+L}{3}}\right)}{\operatorname{scosh}\left(\sqrt{\frac{s+L}{3}}\right)}. \tag{A11}$$

The evaluation of residues for Equation (A11) begins at $s = 0$, where a simple pole is identified. Further, solving Equation $\cosh\left(\sqrt{\frac{s+L}{3}}\right) = 0$ reveals infinitely many poles, given by $s_n = -3\frac{(2n+1)^2\pi^2}{4} - 3L, \quad \text{for } n = 0, 1, 2, \ldots$.

$$\operatorname{Res}\left[\frac{\cosh\left(\chi\sqrt{\frac{s+L}{3}}\right)}{s\cosh\left(\sqrt{\frac{s+L}{3}}\right)}\right] = \left[\frac{\cosh\left(\chi\sqrt{\frac{s+L}{3}}\right)}{s\cosh\left(\sqrt{\frac{s+L}{3}}\right)}\right]_{s=0} + \left[\frac{\cosh\left(\chi\sqrt{\frac{s+L}{3}}\right)}{s\cosh\left(\sqrt{\frac{s+L}{3}}\right)}\right]_{s=s_n}, \tag{A12}$$

at $s = 0$,

$$\operatorname{Res}\left[\frac{\cosh\left(\chi\sqrt{\frac{s+L}{3}}\right)}{s\cosh\left(\sqrt{\frac{s+L}{3}}\right)}\right]_{s=0} = \frac{\cosh\left(\chi\sqrt{\frac{L}{3}}\right)}{\cosh\left(\sqrt{\frac{L}{3}}\right)}, \tag{A13}$$

residue at s_n

$$\operatorname{Res}\left[\frac{\cosh\left(\chi\sqrt{\frac{s+L}{3}}\right)}{s\cosh\left(\sqrt{\frac{s+L}{3}}\right)}\right]_{s=s_n} = -\pi\sum_{n=0}^{\infty}\frac{(2n+1)\cos\left(\frac{(2n+1)\pi}{2}\chi\right)e^{-3\tau\left(\frac{(2n+1)^2\pi^2}{4}+L\right)}}{\left(\frac{(2n+1)^2\pi^2}{4}+L\right)\sin\left(\frac{(2n+1)\pi}{2}\right)}. \tag{A14}$$

The concentration of carbohydrate substrate can be derived by summing Equations (A13) and (A14), as given in Equation (19). Likewise, the semi-analytical expressions for oxygen and product can also be derived using the LHPM method, and the resulting expressions are presented in Equations (21) and (20).

References

1. Iqbal, J.; Iqbala, S.; Muller, C.E. Advances in immobilized enzyme microbioreactors in capillary electrophoresis. *Analyst* **2013**, *138*, 3104–3116. [CrossRef]
2. Baronas, R.; Kulys, J.; Petkevičius, L. Modeling carbohydrates oxidation by oxygen catalyzed by bienzyme glucose dehydrogenase/laccase system immobilized into microreactor with carbon nanotubes. *J. Math. Chem.* **2021**, *59*, 168–185. [CrossRef]
3. Maria, G. Enzymatic reactor selection and derivation of the optimal operation policy, by using a model-based modular simulation platform. *Comput. Chem. Eng.* **2012**, *36*, 325–341. [CrossRef]
4. Tischer, W.; Wedekind, F. Immobilized enzymes: Methods and applications. In *Biocatalysis—From Discovery to Application*; Fessner, W.D., Ed.; Springer: Berlin/Heidelberg, Germany, 1999; Volume 200, pp. 95–126.
5. Khan, A.Y.; Noronha, S.B.; Bandyopadhyaya, R. Glucose oxidase enzyme immobilized porous silica for improved performance of a glucose biosensor. *Biochem. Eng. J.* **2014**, *91*, 78–85. [CrossRef]
6. Doran, P.M. *Bioprocess Engineering Principles*; Elsevier: New York, NY, USA, 1995.
7. Villadsen, J. Principles of metabolic engineering. *Biotechnol. Bioeng.* **2009**, *3*, 226–256.
8. Al-Shannag, M.; Al-Qodah, Z.; Herrero, J.; Humphrey, A.J.; Giralt, F. Using a wall-driven flow to reduce the external mass-transfer resistance of a bio-reaction system. *Biochem. Eng. J.* **2008**, *39*, 554–565. [CrossRef]
9. Carvalho, S.C.; Senra, T.O.S.; Silva, M.M.C.; Aguiar, L.G.; Ferreira, A.L.G. Mathematical modeling of the reactions involved in biodiesel production from waste oils and fats in a batch reactor. *Biofuels* **2025**, *16*, 150–154. [CrossRef]
10. Kushwaha, J.P.; Ahuja, S.; Singh, N.; Kaur, R. Mathematical modeling and kinetics of batch and continuous electro-catalytic oxidation of pharmaceutical-contaminated wastewater. *J. Environ. Manag.* **2024**, *370*, 122871.
11. Karthikeyan, C.; Kumar, V.P.; Preetha, V.; Arakkal, F. Mathematical modeling of a batch reactor and a non-isothermal CSTR with their respective simulation using MATLAB and ASPEN PLUS. In *Chemical Engineering Essentials 2: Advanced Processes, Materials, and Sustainability*; Elsevier: Amsterdam, The Netherlands, 2025; pp. 63–78.
12. Mallikarjuna, M.; Senthamarai, R. Mathematical analysis of batch reactor performance for the enzymatic synthesis of cephalexin: Laplace Homotopy perturbation method and Adomian decomposition method. *Partial Differ. Equ. Appl. Math.* **2024**, *11*, 100806. [CrossRef]

13. Mohammed, A.E.; Mohammed, W.T.; Gheni, S.A. Scale-up of oxidative desulfurization for sour diesel fuel: Modeling, simulation, and reactor design using Fe/AC catalyst. *Case Stud. Chem. Environ. Eng.* **2025**, *11*, 101024. [CrossRef]
14. Daniel, S.; Mallikarjuna, M.; Senthamarai, R. Mathematical modeling and analysis of immobilized glucose dehydrogenase reactions in spherical microreactors. *Eur. J. Pure Appl. Math.* **2025**, *18*, 6203. [CrossRef]
15. He, J.H.; Jiao, M.L.; Gepreel, K.A.; Khan, Y. Homotopy perturbation method for strongly nonlinear oscillators. *Math. Comput. Simul.* **2023**, *204*, 243–258.
16. He, J.H. Homotopy perturbation method: A new nonlinear analytical technique. *Appl. Math. Comput.* **2003**, *135*, 73–79. [CrossRef]
17. Suganya, G.; Senthamarai, R. Analytical approximation of a nonlinear model for pest control in coconut trees by the homotopy analysis method. *Comput. Res. Model.* **2022**, *14*, 1093–1106. [CrossRef]
18. He, J.H. Variational iteration method—A kind of non-linear analytical technique: Some examples. *Int. J. Non-Linear Mech.* **1999**, *34*, 699–708.
19. He, C.H.; Shen, Y.; Ji, F.Y.; He, J.H. Taylor series solution for fractal Bratu-type equation arising in electrospinning process. *Fractals* **2020**, *28*, 2050011. [CrossRef]
20. Madani, M.; Fathizadeh, M.; Khan, Y.; Yildirim, A. On the coupling of the homotopy perturbation method and Laplace transformation. *Math. Comput. Model.* **2011**, *53*, 1937–1945. [CrossRef]
21. Mallikarjuna, M.; Guirao, J.L.G.; Senthamarai, R. Theoretical analysis of amperometric biosensor with substrate and product inhibition involving non-Michaelis-Menten kinetics. *MATCH Commun. Math. Comput. Chem.* **2025**, *93*, 319–347.
22. Sivakumar, M.; Mallikarjuna, M.; Senthamarai, R. A kinetic non-steady state analysis of immobilized enzyme systems with external mass transfer resistance. *AIMS Math.* **2024**, *9*, 18083–18102. [CrossRef]
23. Johnston, S.J.; Hossein, J.; Moshokoa, S.P.; Ariyan, V.M.; Baleanu, D. Laplace homotopy perturbation method for Burgers equation with space- and time-fractional order. *Open Phys.* **2016**, *14*, 247–252. [CrossRef]
24. Owolabi, K.M.; Pindza, E.; Karaagac, B.; Gulay, O. Laplace transform homotopy perturbation method for fractional time diffusive predator–prey models in ecology. *Partial Differ. Equ. Appl. Math.* **2024**, *9*, 100607. [CrossRef]
25. Aljahdaly, N.H.; Alweldi, A.M. On the modified Laplace homotopy perturbation method for solving damped modified Kawahara equation and its application in a fluid. *Symmetry* **2023**, *15*, 394. [CrossRef]

Disclaimer/Publisher's Note: The statements, opinions and data contained in all publications are solely those of the individual author(s) and contributor(s) and not of MDPI and/or the editor(s). MDPI and/or the editor(s) disclaim responsibility for any injury to people or property resulting from any ideas, methods, instructions or products referred to in the content.